ELSEVIER

Journal of Fluids and Structures 19 (2004) 1031–1048

JOURNAL OF FLUIDS AND STRUCTURES

www.elsevier.nl/locate/jnlabr/yjfls

Flow around a porous cylinder subject to continuous suction or blowing

J.H.M. Fransson[a,*], P. Konieczny[b], P.H. Alfredsson[a]

[a]*KTH Mechanics, SE-100 44, Stockholm, Sweden*
[b]*Institut de Mécanique des Fluides de Toulouse, Allée du Pr. Camille Soula, F-31400 Toulouse, France*

Received 20 June 2003; accepted 23 June 2004
Available online 2 October 2004

Abstract

In the present experimental investigation the surface pressure distribution, vortex shedding frequency, and the wake flow behind a porous circular cylinder are studied when continuous suction or blowing is applied through the cylinder walls. It is found that even moderate levels of suction/blowing ($\lesssim 5\%$ of the oncoming streamwise velocity) have a large impact on the flow around the cylinder. Suction delays separation contributing to a narrower wake width, and a corresponding reduction of drag, whereas blowing shows the opposite behaviour. Both uniform suction and blowing display unexpected flow features which are analysed in detail. Suction shows a decrease of the turbulence intensity throughout the whole wake when compared with the natural case, whilst blowing only shows an effect up to five diameters downstream of the cylinder. The drag on the cylinder is shown to increase linearly with the blowing rate, whereas for suction there is a drastic decrease at a specific suction rate. This is shown to be an effect of the separation point moving towards the rear part of the cylinder, similar to what happens when transition to turbulence occurs in the boundary layer on a solid cylinder. The suction/blowing rate can empirically be represented by an effective Reynolds number for the solid cylinder, and an analytical expression for this Reynolds number representation is proposed and verified. Flow visualizations expose the complexity of the flow field in the near wake of the cylinder, and image averaging enables the retrieval of quantitative information, such as the vortex formation length.

1. Introduction

The phenomenon of vortex shedding from bluff bodies still remains a challenging and interesting problem. The canonical configuration of the motion of a fluid past a circular cylinder is of relevance to a large number of flows found in industrial applications (the flow past moving vehicles, pylons of bridges, buildings, etc.), as well as in natural settings. Recently, interest has been focussed on the ability to manipulate the wake of a bluff body to reduce drag, increase heat transfer or mixing, and enhance combustion.

There is an abundance of studies in the literature on the flow past a circular cylinder, starting with Strouhal (1878) and Kármán (1912). A complete overview of the field will not be attempted here; for the interested reader there are

*Corresponding author. Tel.: +46-8-790-7624; fax: +46-8-790-7654.
E-mail addresses: jens.fransson@mech.kth.se (J.H.M. Fransson), hal@mech.kth.se (P.H. Alfredsson).

0889-9746/$ - see front matter © 2004 Elsevier Ltd. All rights reserved.
doi:10.1016/j.jfluidstructs.2004.06.005

several recent reviews available, [e.g., Williamson (1996), Buresti (1998) and Norberg (2003)], as well as a comprehensive two volume monograph (Zdravkovich, 1997, 2003).

The characteristics of the flow around a cylinder depend strongly on the cylinder Reynolds number ($\mathrm{Re} = U_\infty D/\nu$, where U_∞ is the free stream velocity, D is the cylinder diameter and ν the fluid kinematic viscosity). Over the past 50 years different flow phenomena have been observed depending on the Re, implying that the accepted definition of various flow regimes has continuously been extended. In Zdravkovich (1997) a collection and summary of the existing flow regimes may be found.

In the present study we focus on Reynolds numbers of the order of 10^4, which is in the subcritical regime (also known as the shear-layer transition regime). In these conditions the boundary layers on the cylinder are still laminar, they separate from the body and instabilities develop. Many studies have been focusing on the subcritical range, e.g., a compilation of more than 70 references can be found in Cantwell and Coles (1983). Although a cylinder mounted perpendicular to the free stream may seem as a simple generic case, the exact flow behaviour may still be influenced by various flow and geometry factors, for instance the turbulence level of the free stream, the surface roughness of the cylinder, the blockage ratio as well as the aspect ratio of the cylinder. For low Reynolds numbers very large aspect ratios are needed to obtain a two-dimensional flow, but for flows in the subcritical range the aspect ratio is less critical [see Norberg (1994)].

1.1. Control of vortex shedding

This section reviews some earlier attempts to control the vortex shedding behind bluff bodies, starting with blunt trailing-edge bodies, continuing with cylinders and porous cylinders. The section ends by declaring the objective of the present study.

1.1.1. Blunt trailing-edge bodies

A control approach that is effective in reducing the average strength of the vortices and the shedding frequency is base bleed [cf., e.g., Bearman (1967); Wood (1967)]. For successively increasing bleeding rates the regular shedding of vortices ceases, intermittently at first, and then completely. Hannemann and Oertel (1989) performed numerical simulations on the effect of uniform blowing from the base at $\mathrm{Re} = 200$, and reported a critical value of the bleed coefficient ($c_q = U_0/U_\infty = 0.214$, where U_0 is the bleed velocity) for which vortex shedding was suppressed. Recently, Arcas and Redekopp (2004) performed a similar simulation, but with a variable base bleed velocity distribution where they reported the critical c_q-Re correlation in the range $200 \leqslant \mathrm{Re} \leqslant 1200$. The critical c_q was shown to asymptote to a constant value (argued to be $\lesssim 0.30$ in most wake flows) for increasing Re. Uniform suction from the base was considered numerically by Hammond and Redekopp (1997) and they reported a continuous decrease of the wake shedding frequency with a gradual increase of suction until an abrupt suppression occurs at a sufficiently high suction rate ($c_q = -0.22$).

1.1.2. Cylinders

For cylinders at low Reynolds numbers (<300) several techniques have been shown to have a potential to suppress vortex shedding or shift the shedding frequency. One such method is to oscillate the cylinder in rotary motion (Berger, 1967) at a suitable frequency and amplitude. Another is to heat the cylinder (Wang et al., 2000) thereby changing the viscosity close to the cylinder surface, giving rise to a change in the effective Reynolds number. A different approach is to use feedback control, as demonstrated in both experiments (Roussopoulos, 1993) and simulations (Park et al., 1994). In the experiments, the actuation was acoustically induced through a loudspeaker (in a wind tunnel) as well as by vibrating the cylinder (in a water channel), whereas in the numerical study blowing and suction slots on the rear part of the cylinder were utilized. No blowing and suction experiments exist for this Reynolds number range (<300) since the size of the cylinder for typical velocities in air or water would be very small and it would almost be impossible to implement such a device at this scale.

For higher Reynolds number flows (larger cylinders) a possible form of (passive) control consists in modifying the geometry in order to affect the vortex shedding. Experiments along this line for flow past a circular cylinder were reported by Roshko (1955, 1961); he simply placed a splitter plate on the centreline behind the cylinder. With a proper length of the splitter plate the flow behaviour can change from the alternating shedding mode to a symmetrical mode, with two closed recirculation regions on each side of the plate.

In the subcritical range of interest in this study, Tokumaru and Dimotakis (1991) carried out experiments on circular cylinders executing forced rotary oscillations. They managed to obtain a significant drag reduction of up to 80% at $\mathrm{Re} = 15\,000$ for certain ranges of frequency and amplitude of the sinusoidal rotary oscillation. Computational results (Shiels and Leonard, 2001) have confirmed these experimental observations and there are indications that this kind of control could be even more efficient at higher Reynolds number.

1.2. Porous cylinders with suction or blowing

Another possibility is flow manipulation through the application of suction or blowing. Early experiments on a porous cylinder made of sintered bronze were carried out by Pankhurst and Thwaites (1950). They made experiments with continuous suction, but also combined suction with a flap in the form of a short splitter plate placed at various angles. At an angle of 180°, i.e., along the downstream symmetry line, and for sufficient suction, the separation is entirely prevented and a remarkably close approximation to the potential flow solution is achieved, as attested by the pressure distribution and by mean flow velocity profiles of the wake. They concluded from their experiments that values of $C_q\sqrt{\mathrm{Re}}$ larger than ≈ 30 were needed to avoid separation.[1] They also reported values of the drag coefficient, but did not do any time-resolved measurements to determine the vortex shedding frequency. Boundary layer measurements on the same porous cylinder were performed by Hurley and Thwaites (1951) and in general good agreement was found with laminar boundary layer theory.

Continuous blowing through the whole surface has also been studied experimentally by Mathelin et al. (2001a, b). The cylinder in these experiments is 16.2 mm in outer diameter and made of sintered stainless-steel, with 30% of porosity and 30 μm average pore diameter [see Mathelin et al., (2001a)] for the detailed description of the set-up. Among the effects observed, they noted the presence of a wider wake and a decrease of the Strouhal number. The decrease in Strouhal number is linear with the injection rate until saturation occurs. For a 5% injection at $\mathrm{Re} = 3900$ the reduction is for example 25%. Taking into account this reduction of the vortex shedding frequency, and the Strouhal–Reynolds curve for low Reynolds number. An analytical flow submitted to blowing would have the same characteristics in terms of instability as a flow at a lower Reynolds number, and an analytical relation was determined to provide the equivalent Reynolds number of the canonical case which produces the same behaviour as the case with blowing.

A different type of blowing can be achieved through the use of synthetic jets, which provide a localized addition of momentum through the surface. Glezer and Amitay (2002) show that synthetic jets on selected positions over the cylinder can give a delay of separation for different Reynolds number (i.e., both for a turbulent and a laminar boundary layer). They argued that this delay was caused by increased mixing within the boundary layer. In addition, the interaction between the jet and the cross flow has a profound effect both on the separated shear layer and on the wake; the magnitude of the Reynolds stresses is reduced indicating that the delay in separation is not merely the result of a transition to turbulence in the boundary layer.

1.3. Present study

The objectives of our study is, partly, to complement the investigations just cited by considering both the effect of uniform suction and blowing on a smooth, porous cylinder. We will document the changes of the flow in the subcritical regime, in terms of mean and fluctuating velocity profiles in the wake through hot-wire anemometry, pressure distributions and vortex shedding for different blowing and suction rates. Smoke visualizations of the flow complement the study providing a clear picture of the flow behaviour under parametric variations. Attention to the effects of free stream turbulence will also be paid, and comparison will be made with the known results of the canonical case for which the behaviour of the critical transition thresholds with free-stream turbulence is known (Kiya et al., 1982).

Finally, it is shown here that the suction/blowing rate empirically can be represented by an effective Reynolds number for the solid cylinder, and an analytical expression for this Reynolds number representation is proposed and verified.

2. Experimental set-ups and flow visualization technique

Most of the experiments were performed in the S4–wind tunnel at IMFT in Toulouse, which is a low-speed closed-circuit tunnel. The dimensions of the test-section are $1800 \times 700 \times 600\,\mathrm{mm}^3$ (length(L) × height(H) × width(W)). The background streamwise disturbance level is 0.5% and 0.1% of the free stream velocity at 2.5 and 25 m/s, respectively. It is provided with a three-dimensional traversing mechanism and allows automatized computer controlled measuring and traversing in one direction (y) with a resolution of $\frac{1}{80}$ mm. Measurements were made with hot-wire anemometry using a single wire Dantec probe, with 5 μm and 1.25 mm in wire diameter and prong separation, respectively. The calibration was done against a Pitot-static tube using the standard King's law as curve fitting, which typically generated a maximum error of 1% from the calibration data, and was carried out on the centreline 400 mm upstream of the cylinder.

[1] Here C_q is a suction coefficient defined as the suction flow rate per unit span divided by ($U_\infty D$).

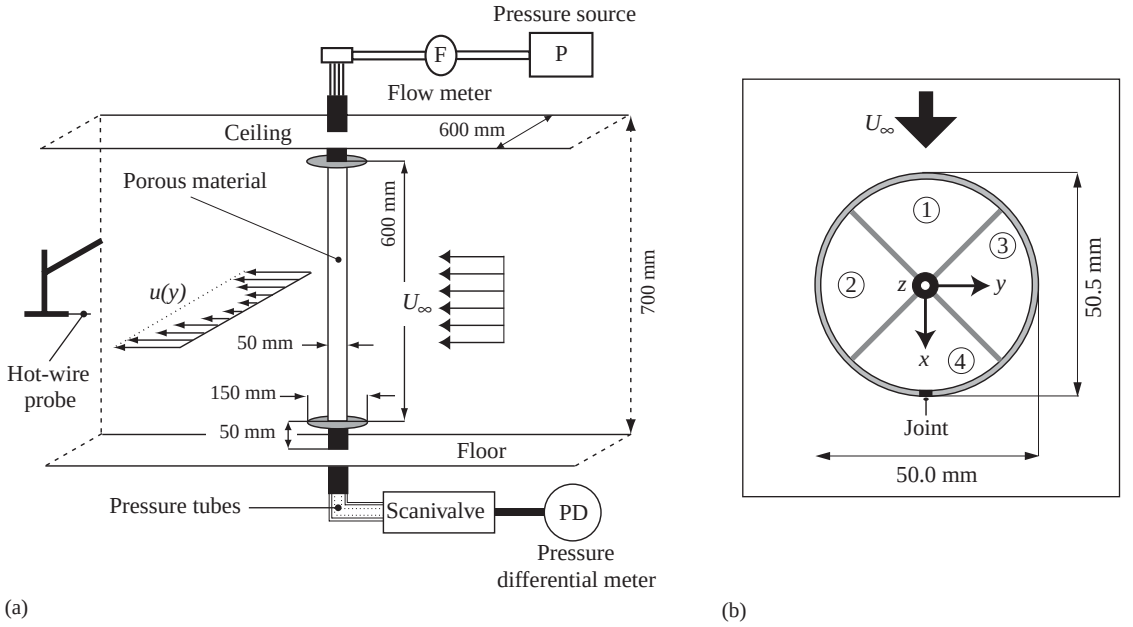

Fig. 1. (a) Experimental set-up of the porous cylinder, and (b) the interior of the cylinder with four separate pressure chambers.

The diameter (D), wall thickness (t) and the porous length of the cylinder were 50, 2.5 and 600 mm, respectively. The end parts of the cylinder are made of brass with four inlets for tube connections. The four tubes from the inlets are then confluenced before connection to a flow meter (rotameter type), which in turn is connected to a pressure source (vacuum cleaner or high pressure air depending on whether suction or blowing is required). The cylinder is mounted vertically in the test-section with end plates located at a distance $\Delta = 50$ mm from the ceiling and floor. This is done to minimize three dimensional end effects that are created from the boundary layers developing on ceiling and floor [cf. Szepessy and Bearman (1992), for a thorough investigation of the effect of end plates]; see Fig. 1(a) for the experimental set-up. The blockage and aspect ratios of this set-up are 0.083 ($= D/W$) and 12 ($= (H - 2\Delta)/D$), respectively.

The inside of the cylinder consists of four isolated chambers, as shown in Fig. 1(b), in order to achieve varying suction rates through different portions of the cylinder, in view of future planned experiments. There are 16 surface pressure taps (inner diameter 0.5 mm) positioned around the cylinder, which are shifted along the length of the cylinder forming a spiralling pattern in order to minimize mutual interference. The pressure holes can be moved relative to the oncoming flow by rotating the cylinder, and the pressure tubings are connected to a Scanivalve to facilitate the measurements. The coordinate system used here has its origin in the centre of the cylinder (see Fig. 1(b) for a definition).

Some of the experiments were also made with a turbulence generating grid placed at the inlet of the test-section. The grid has a mesh width of 25 mm and the bars are of rectangular cross-section with a width and a thickness of 4 and 3 mm, respectively.

2.1. Characteristics of the porous material

The porous cylinder is made of a sintered plastic material with an average pore size of 16 μm. Previous surface roughness measurements on a similar but flat porous plate (Fransson and Alfredsson, 2003) show a roughness height of about 2 μm. For the present case the surface can be considered to be hydraulically smooth. The cylinder is made from a flat plate which is bent to form a circular cylinder. This means that there is a joint in the axial direction along the whole cylinder, and this gives rise to a small asymmetry with a 0.5 mm larger diameter in average when measured over the joint, see Fig. 1(b). The joint is therefore in most cases positioned 180° away from the oncoming flow in order to avoid imposing a flow asymmetry.

To determine the permeability of the material the pressure difference (ΔP) over the cylinder wall and the flow rate ($Q = V \times S$, where V and S are the velocity through the porous material and the surface area, respectively) are measured, when suction is applied. Through Darcy's law the permeability (k) is then determined to be $k = \mu t V/\Delta P = 2.3 \times 10^{-7}\,\mathrm{m}^2$, by best line fitting to the data (μ is the dynamic viscosity).

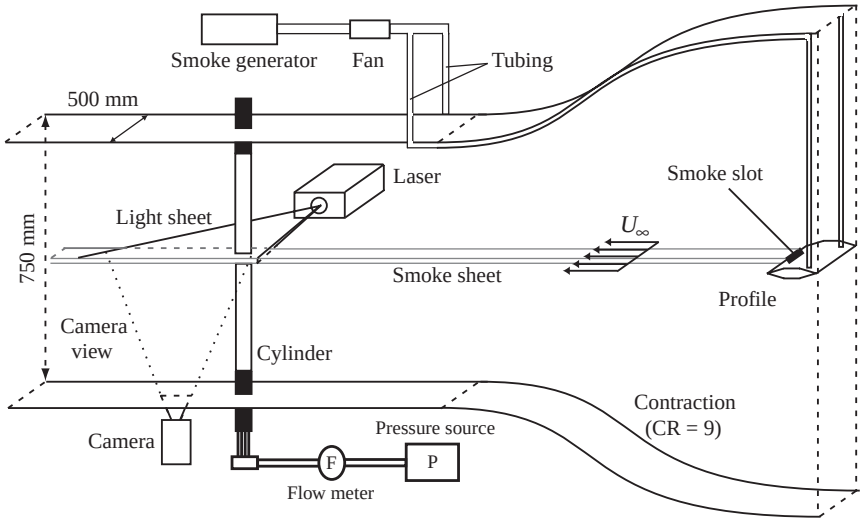

Fig. 2. Flow visualization set-up of the porous cylinder.

2.2. Flow visualization technique

The flow visualizations were carried out in the BL–wind tunnel at KTH Mechanics. For all technical information about this wind tunnel the interested reader is referred to Lindgren and Johansson (2002).

For the flow visualizations the same cylinder set-up was used as for the hot-wire and pressure measurements (with a new porous cylinder section because of transport damages from France to Sweden, and without end plates to avoid camera view reduction) and in Fig. 2 the flow visualization set-up is shown. A horizontal smoke sheet was created by injecting smoke through a slot in a wing-profile, which was located over the whole spanwise distance in the stagnation chamber of the wind tunnel. The profile has two tubing inlets, one on each side close to the walls. The smoke was generated by heating glycol-based liquid with a disco smoke generator, JEM ZR20 Mk II, and forced by a small fan through the tubing into the profile enabling a steady leakage of smoke through the slot.

The light source was a continuous Ar-ion laser, LEXEL 95–4, which gave the high light intensity needed for the short camera shutter times. The laser beam (1.5 W) was aligned through a cylinder lens creating a light sheet intersecting with the smoke sheet from the side (perpendicular to the flow field and the test-section). The collection of flow visualization images was taken with a digital video camera (SONY TRV900 with 576×720 pixels) with a shutter time of 2 ms and with a rate of 20 images per second.

3. Measurement results

In the present work, the cylinder Reynolds number ($\mathrm{Re} = U_\infty D/\nu$) is kept constant at $\mathrm{Re} = 8300$ unless otherwise stated, whereas the suction and blowing rates are varied. This rate is expressed through the parameter $\Gamma = (V/U_\infty) \times 100$, where V is the velocity through the porous material, negative for suction and positive for blowing, and U_∞ is the oncoming streamwise velocity. At $\mathrm{Re} = 8300$ the oncoming mean flow velocity is $U_\infty = 2.5\,\mathrm{m/s}$ and the range of Γ investigated in this section is $-4 < \Gamma < 6$. The Reynolds number would, for the case of a solid cylinder, produce a laminar boundary layer and separation with a turbulent wake.

3.1. Suction and blowing distributions

Since the surface pressure distribution varies around the circumference of the cylinder, when exposed to an oncoming flow, this gives a nonuniform suction/blowing if the pressure inside the cylinder is constant. This is the case when the chambers are connected to a single tube through which suction/blowing is performed. A possible remedy to obtain uniform velocity at the surface is to divide the inner part of the cylinder into a large number of chambers that are individually regulated; this, however, would be an inpractical solution. In the present experiments, the four chambers are connected to the same tubing, and hence have the same pressure. For the suction case, the largest suction velocity occurs along the front stagnation line and then it decreases towards the rear. In the separated region the suction velocity

is fairly constant and for $\Gamma = -1.4$ the suction velocity is about 6% smaller in this region as compared to the front. For larger suction rates the difference becomes smaller. In contrast, for the blowing case the smallest blowing velocity is along the frontal stagnation line and then increases and becomes constant from about 65° and downwards. In this case the maximum variation is less than 6% and also here the variation decreases with increasing Γ. The suction/blowing rate distributions were calculated from the static pressure measurements on the cylinder surface together with the measured total flow rate through the material and the measured permeability.

The uniformness of the transpiration velocity along the cylinder was checked by measuring the static pressure (which remained constant) in the chambers at different positions along the cylinder axis. This was done by sliding a tiny tube through holes in the end cap of the cylinder.

3.2. Effect of suction/blowing on the pressure distribution

Simply by analysing the change of the surface pressure distribution when the cylinder is subject to continuous blowing or suction, one can draw some important conclusions.

In Fig. 3(a) the effect of different Γ-values on the C_p-distribution is shown and compared with the potential flow solution (dash-dotted line). Three main remarks can be made; firstly, one can observe how $C_{p,\min}$ is reduced down to a value close to -2 for $\Gamma = -2.6$ and tends to -1 for $\Gamma = +2.6$; secondly the separation point (ϕ_s) moves towards higher angles from the centreline ($\phi_s \approx 105^\circ$ for $\Gamma = -2.6$), and when blowing is applied, the flow is seen to separate at lower angles; thirdly the base pressure coefficient ($C_{p,B}$) is increased for the case of suction producing a significant increase in the adverse pressure recovery ($C_{p,B} - C_{p,\min}$), whilst for the case of sufficiently large blowing rates, the recovery region is eliminated.

The inflection point (IP) region on the C_p-curve, marked with a dashed ellipse in Fig. 3(a), is often used to estimate the location of the separation point and this is the criterion employed in the preceding paragraph. Suction makes the boundary layer profile fuller and hence more resistant to separation, in analogy with high Reynolds number flow. At $\mathrm{Re} \sim 10^5$ transition in the boundary layer occurs (the exact Re-value depends on the flow quality and the surface roughness) and the separation point moves from the front part of the cylinder to the rear part, due to the turbulent boundary layer that can make the flow adhere longer to the surface. In Fig. 3(b) the free stream velocity is increased ten times and the C_p-distribution is compared with results when a turbulence intensity ($\mathrm{Tu} = u_{\mathrm{rms}}/U_\infty$) of 3% is present (causing transition in the boundary layer at subcritical Reynolds numbers); this was done by mounting a turbulence generating grid at the inlet of the test-section. It is clearly seen, by comparing the (○)-symbols in Fig. 3(a) with the (✻)-symbols in (b), that suction and high levels of free stream turbulence have a similar influence on the C_p-distribution. Furthermore, in (b), one can observe how a small blowing/suction rate ($\Gamma = \pm 0.4$) effects the location of $C_{p,\min}$ and consequently the separation point, but not the base pressure coefficient.

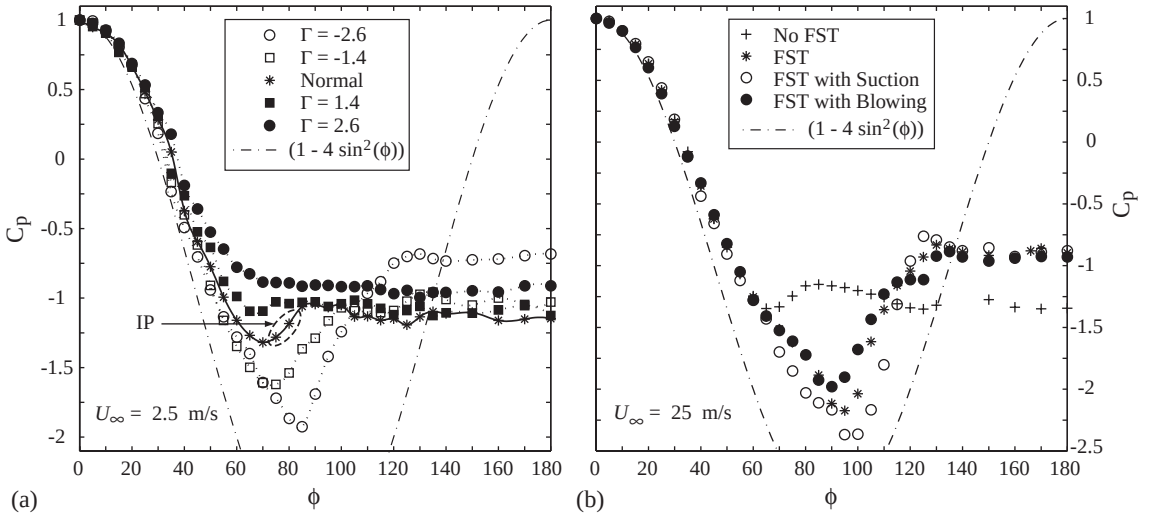

Fig. 3. The pressure distribution around the cylinder is shown for different Γ-values. (a) shows the effect of blowing/suction with a laminar oncoming flow ($U_\infty = 2.5\,\mathrm{m/s}$, $\mathrm{Re} = 8300$, $\mathrm{Tu} = 0.5\%$) and (b) shows the effect of free-stream turbulence generated by a turbulence generating grid, the blowing/suction is $\Gamma = \pm 0.4$ ($U_\infty = 25\,\mathrm{m/s}$, $\mathrm{Re} = 83\,000$, $\mathrm{Tu} = 3\%$). Dash-dotted line is the potential flow solution.

3.3. Effect of suction/blowing on the surrounding flow

In Fig. 4 the mean velocity profiles for the normal case ($\Gamma = 0$), one suction case ($\Gamma = -2.6$), and one blowing case ($\Gamma = +2.6$) are plotted across the wake for different x/D-positions (see caption for symbols). Close to the cylinder (x/D small), one can observe the presence of negative values of the velocity (i.e., speeds higher than the free stream velocity). This is the effect of the shoulder acceleration around the cylinder, which for higher x/D-values is seen to disappear and the profiles approaches the Schlichting's far wake shape [see, e.g., Zdravkovich (1997), Chapter 9.7]. For the blowing case the shoulder acceleration is, however, quite persistent and may be observed down to $x/D = 3$.

When suction is applied, the velocity decreases close to the cylinder compared to the normal case, but farther away it actually becomes larger. This is due to the presence of low speed regions in the normal case, as shown in Fig. 5 for

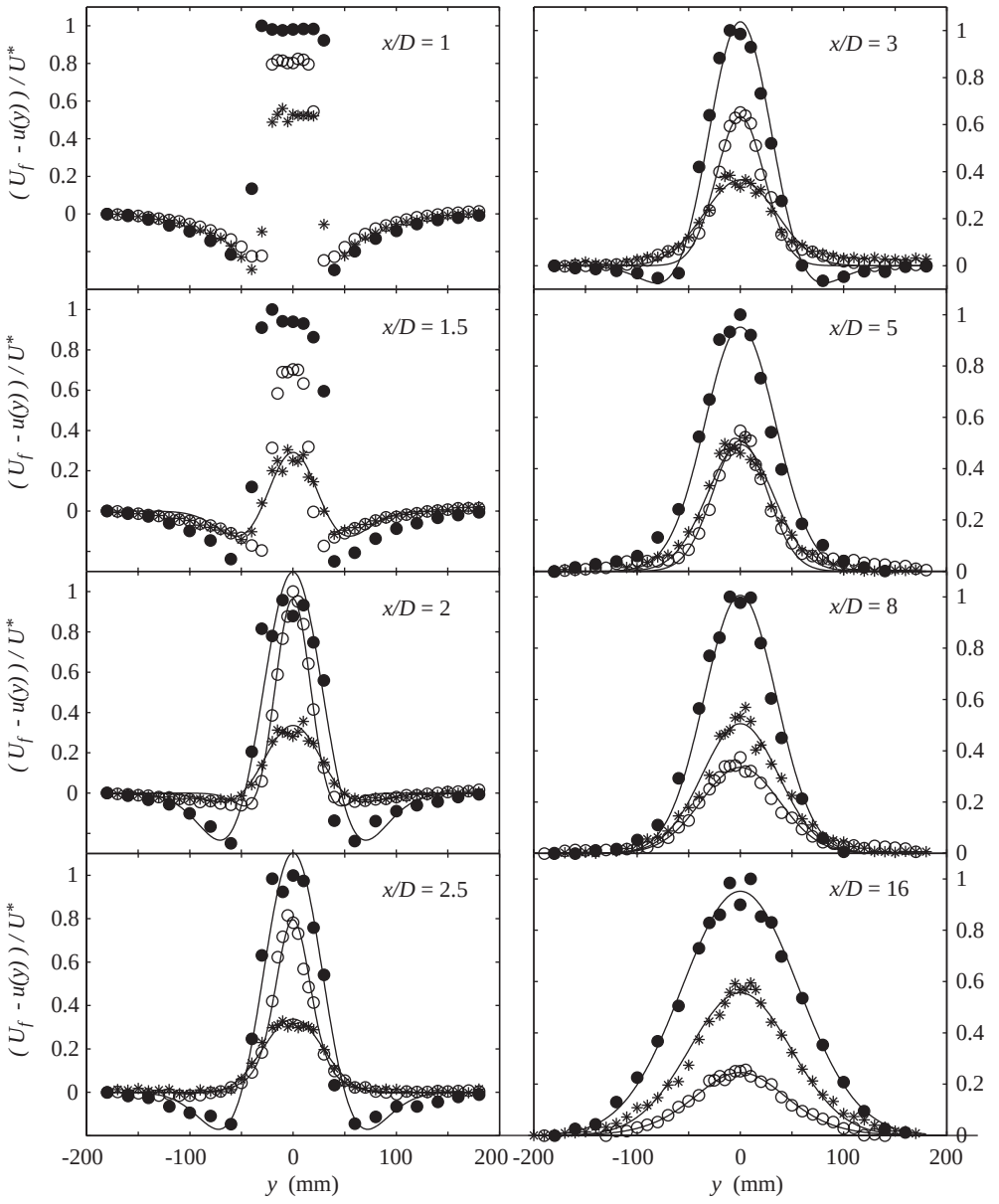

Fig. 4. Mean velocity profiles at different positions behind the cylinder for the normal, the suction, and the blowing case. (∗,○,●) denotes $\Gamma = (0, -2.6, +2.6)$. U_f is the mean velocity far from the cylinder in the y-direction and $U^* = \max(U_f - u(y))$ for all Γ and changes with the x/D-position. The solid lines are curve fits to data.

$\Gamma = 0$, where the contours represent the mean streamwise velocity normalized with U_∞. The dotted, dash-dotted, dashed, and solid contour lines correspond to $u/U_\infty = 0.8$, 0.9, 1.0, and 1.1, respectively. The grey regions correspond to $u_{\rm rms}/U_{\rm local} \geqslant 0.30$, which is a zone that has to be considered with caution since the hot-wire results may be significantly affected by large flow angles and even backflow. Note that some of the profiles in Fig. 4 also become affected. For successively decreasing Γ (increasing suction) the mean streamwise velocity behind the cylinder decreases at first, but at $\Gamma \approx -2.6$ there is a sudden change of trend and the velocity starts to increase. This can be observed in the contour plots of Fig. 5. The reason for a sudden change in the mean velocity component is the fact that suction affects the boundary layer around the cylinder and delays the separation as pointed out earlier. A possible explanation is that suction also stabilizes the wake and that less mixing occurs. With increasing suction the separation point on the cylinder is moved from the front to the rear part of the cylinder implying a decrease of the shoulder acceleration (see Fig. 5), a narrower wake, and thereby an increase of the velocity in the wake. For very high suction rates the flow would stay attached to the cylinder giving rise to a potential-like solution, and hence the wake will be less pronounced. This hypothesis is corroborated by inspection of Fig. 3(a).

Contrary to suction, blowing causes the flow to separate earlier, also observed in Fig. 3(a). Despite the direct injection of air behind the cylinder the effect of the separation point is much larger and the mean velocity is reduced in the wake. Increasing blowing widens the wake and the shoulder acceleration is seen to amplify leaving low speed fluid close behind the cylinder as the wake grows. This can be observed in Fig. 5.

In Fig. 6, $u_{\rm rms}$-profiles corresponding to the mean velocity profiles in Fig. 4 are shown, whereas Fig. 7 displays the contour plots of the turbulence intensity (Tu) for different values of Γ. Solid, dashed, dash-dotted, and dotted contour lines correspond to $\mathrm{Tu} = u_{\rm rms}/U_\infty = 0.02$, 0.04, 0.06, and 0.08, respectively. Gray-filled regions are the same as in Fig. 5 ($u_{\rm rms}/U_{\rm local} \geqslant 0.30$), and the quantitative results in these regions should be viewed with caution. Note that some of the profiles in Fig. 6 also become affected. The Tu-level consistently decreases for increasing suction and it is possible to discern a more narrow wake. Furthermore, one can observe a strengthened formation of the two-peak disturbance distribution across the wake, which are seen to move towards the cylinder for increasing suction (see also Fig. 6). When blowing is applied the Tu-level is reduced close to the cylinder (Fig. 7). This may be due on the one hand to the fact that the size of the large scale eddies are enhanced, and therefore less mixing occurs close to the cylinder, and on the other hand due to the introduction of low velocity fluid through the surface.

In Fig. 8 the turbulence intensity Tu is plotted along the centreline (CL) behind the cylinder for different Γ. The low Tu-level close to the cylinder when blowing is applied is well illustrated in Fig. 8(b) (as discussed in the last paragraph). It is clearly shown that blowing only effects the very near wake up to $x = 250\,\mathrm{mm}$ ($5D$) (cf. Fig. 8b), whilst suction has a persisting stabilizing effect on the flow behind the cylinder (cf. Fig. 8a).

In Fig. 8(c) some of the Tu_{CL}-data in Figs. 8(a) and (b) are used together with other data to show the independence of different x/D-positions on blowing/suction (Γ). The Tu_{CL}-data are normalized with $Tu_{CL}^{\Gamma=0}$ and decay linearly with increasing suction for any fixed x/D-position, whereas the blowing has no effect from $x/D = 5$ and forward.

An additional way to illustrate the widening and narrowing of the wake is through the flatness ($F = \overline{(u-\overline{u})^4}/\overline{u^2}^2$) evolution, since one would expect high intermittency peaks at the wake edge (laminar/turbulent edge). In Fig. 9 the

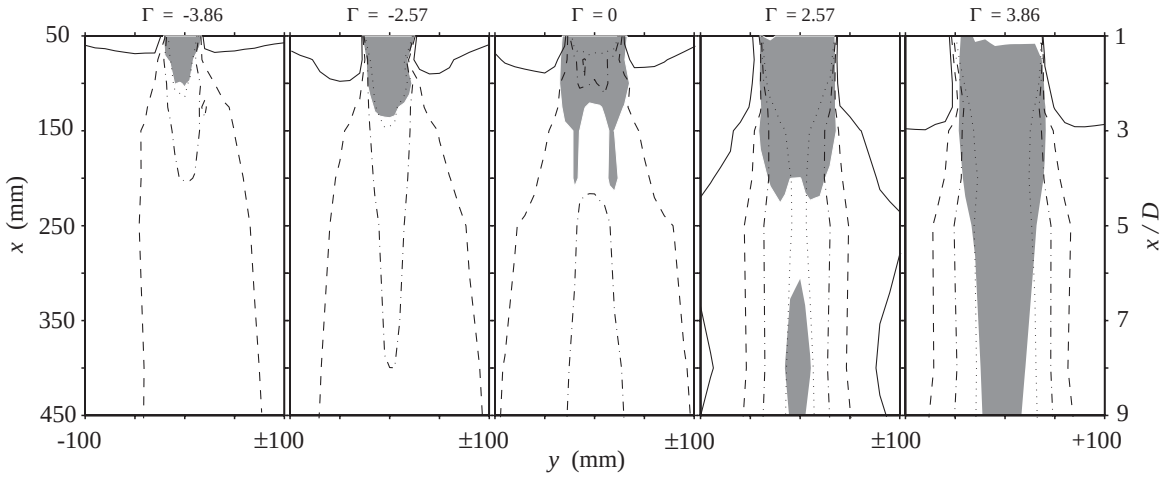

Fig. 5. Contour plots of $u(x,y)/U_\infty$ in the xy-plane. Dotted, dash-dotted, dashed, and solid contour lines correspond to $u/U_\infty = 0.8$, 0.9, 1.0, and 1.1, respectively. Grey-filled regions correspond to $u_{\rm rms}/U_{\rm local} \geqslant 0.30$.

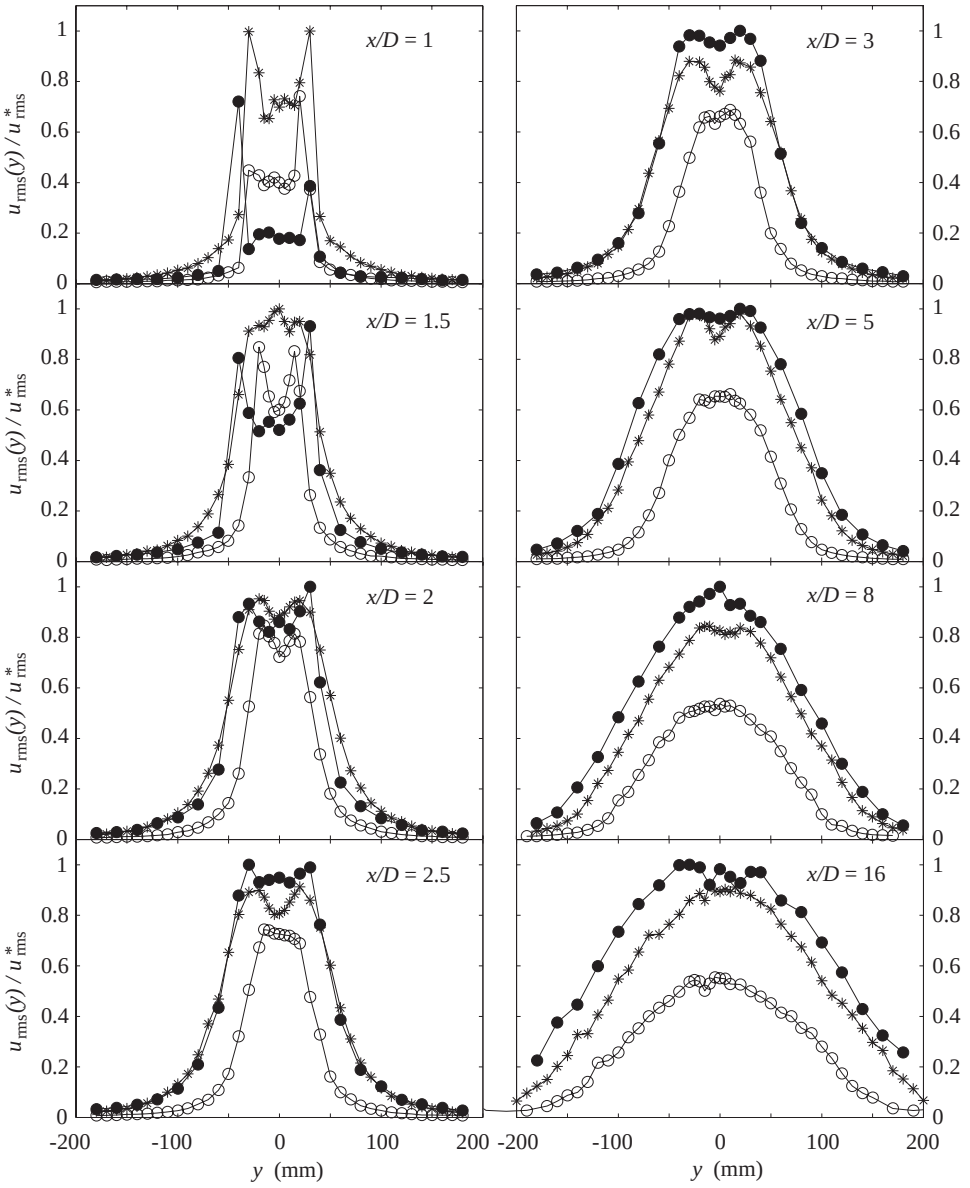

Fig. 6. u_{rms}-profiles at different positions behind the cylinder for the normal, the suction, and the blowing case. (✻,○,●) denotes $\Gamma = (0, -2.6, +2.6)$. u^*_{rms} is max(u_{rms}) for all Γ and changes with the x/D-position.

flatness is plotted for the three cases at different downstream positions. From this figure one can clearly see a trend of earlier departure of the F-values from the centre with suction, and a corresponding delay (however not as clear) with blowing, compared to the normal case. The peak level difference between the three cases can be explained by an amplitude increase of the vortex shedding frequency when suction is applied and vice versa for the blowing case. The peak in F for the suction case is clearly seen to appear close to the centre, corresponding to a narrower wake. This narrowing and widening could also be observed directly from the profiles in Fig. 4 and from the contour plots in Fig. 6. The error in calculating the flatness due to rectification seems to be small. The questionable data in the profiles are found within $1.5D$ centred around the wake symmetry axis. The data corresponding to the normal and the suction cases at $x/D = 4$ and 8 are unaffected while the region width of possibly affected data decreases with x/D in the blowing case (cf. Figs. 5 or 7).

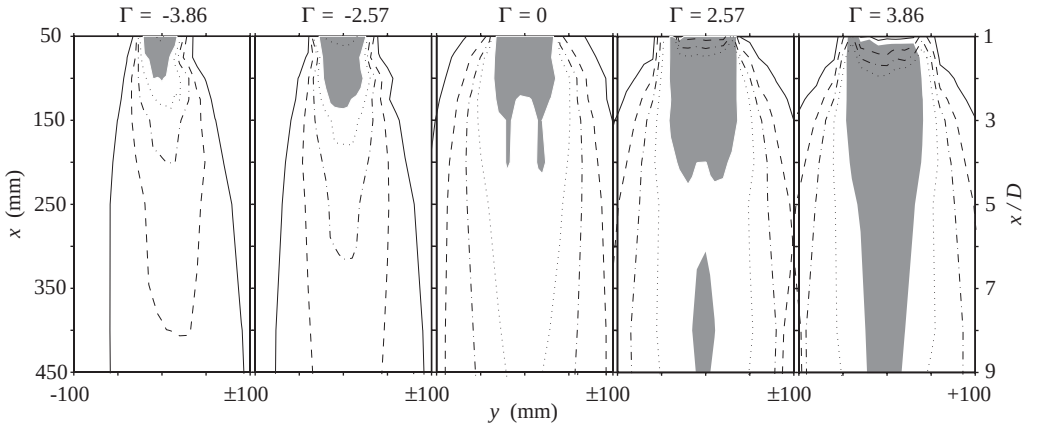

Fig. 7. Shows contour plots of Tu in the xy-plane. Solid, dashed, dash-dotted, and dotted contour lines correspond to $\mathrm{Tu} = u_{\mathrm{rms}}/U_\infty = 0.02$, 0.04, 0.06, and 0.08, respectively. Grey-filled regions correspond to measured values of $u_{\mathrm{rms}}/U_{\mathrm{local}} \geqslant 0.30$.

3.4. Effect on the vortex shedding frequency

Applying continuous blowing or suction can be interpreted as a decrease or increase, respectively, of an effective Reynolds number (related to an effective diameter), which is in contrast to intuition. This is demonstrated in the following section, where a function of an effective Reynolds number ($\mathrm{Re}_{\mathrm{eff}}$) versus the parameter Γ is searched for in a similar manner as Mathelin et al. (2001b), but including suction ($\Gamma < 0$) and therefore valid in a wider Re-range.

In Fig. 10(a) several different data collections of the Strouhal number ($\mathrm{St} = f_K D/U_\infty$, where f_K is the von Kármán vortex shedding frequency) are shown versus the Reynolds number. The first five data sets plotted here are taken from the collected work by Norberg (2003) (his Fig. 1) and the remaining from Zdravkovich (1997) (his Fig. 13.9), to where the interested reader is referred for complete references. The huge amount of data are here used in order to get a robust curve fit, insensitive to free-stream turbulence, blockage, and aspect ratio. If one assumes a constant value of St ($\lesssim 0.2$) in a wide range of Re one can fit an σth degree Re-curve (two terms) to the data according to:

$$\mathrm{St}(\mathrm{Re}) = m + n[\log_{10}(\mathrm{Re}) + k]^\sigma. \tag{1}$$

In Table 1 all the parameters used in this and the following curve fits are given. Furthermore, in Fig. 10(b) St is plotted versus Γ from the present measurements, where both U_∞ and V are varied and Re is in the range $8.5\text{–}25 \times 10^3$. For the collection of those data the probe was positioned approximately one diameter downstream of the cylinder and outside the shear layer. The f_K is determined by selecting the frequency, where the distinct energy peak appears in the power spectrum. The more suction/blowing is applied, the more diffuse becomes this energy peak (which is in accordance with Re-dependent results both for high and low Re), however in Fig. 10(b) only data where a distinct frequency can be detected are shown. From this figure it is seen that suction increases the St of about 50% for $\Gamma \approx -2.5$. In contrast to suction, blowing decreases the St with around 25% for $\Gamma \approx +5$ [in agreement with Mathelin et al. (2001b)], i.e., the effect on the absolute change is smaller than for suction.

An analytical expression of $\mathrm{Re}_{\mathrm{eff}}(\Gamma)$ can be derived by making use of Eq. (1) and after assuming the following relation between St and Γ:

$$\mathrm{St}(\Gamma) = d + \frac{\mathrm{e}^{a(\Gamma+e)} - \mathrm{e}^{b(\Gamma+e)}}{c}. \tag{2}$$

The curve fit in Fig. 10(b) is done with Eq. (2). After simple manipulations of the equation $\mathrm{St}(\mathrm{Re}) = \mathrm{St}(\Gamma)$ (Eqs. (1) and (2)), the expression of $\mathrm{Re}_{\mathrm{eff}}(\Gamma)$ can be written as

$$\log_{10}(\mathrm{Re}_{\mathrm{eff}}(\Gamma)) = -k \pm \mathrm{abs}\left\{\left(\Delta S - m + d + \frac{2}{c}\exp\left[(\Gamma+e)\frac{(a+b)}{2}\right]\sinh\left[(\Gamma+e)\frac{(a-b)}{2}\right]\right)/n\right\}^{1/\sigma} \tag{3}$$

and is plotted in Fig. 10(c). Here ΔS is the needed Strouhal shift for an equal value of the Eqs. (1) and (2) with $\mathrm{Re} \sim 10^3 - 10^4$ and $\Gamma = 0$, respectively. The (+)-sign in Eq. (3) is for $(\Delta S - m + \mathrm{St}(\Gamma)) > 0$ and the (−)-sign for $(\Delta S - m + \mathrm{St}(\Gamma)) < 0$. Note, that the relation between $\mathrm{Re}_{\mathrm{eff}}$ and Γ described by Eq. (3) spans a large range of Reynolds numbers, i.e., from $\mathrm{Re} \sim 10^2$ to 10^6.

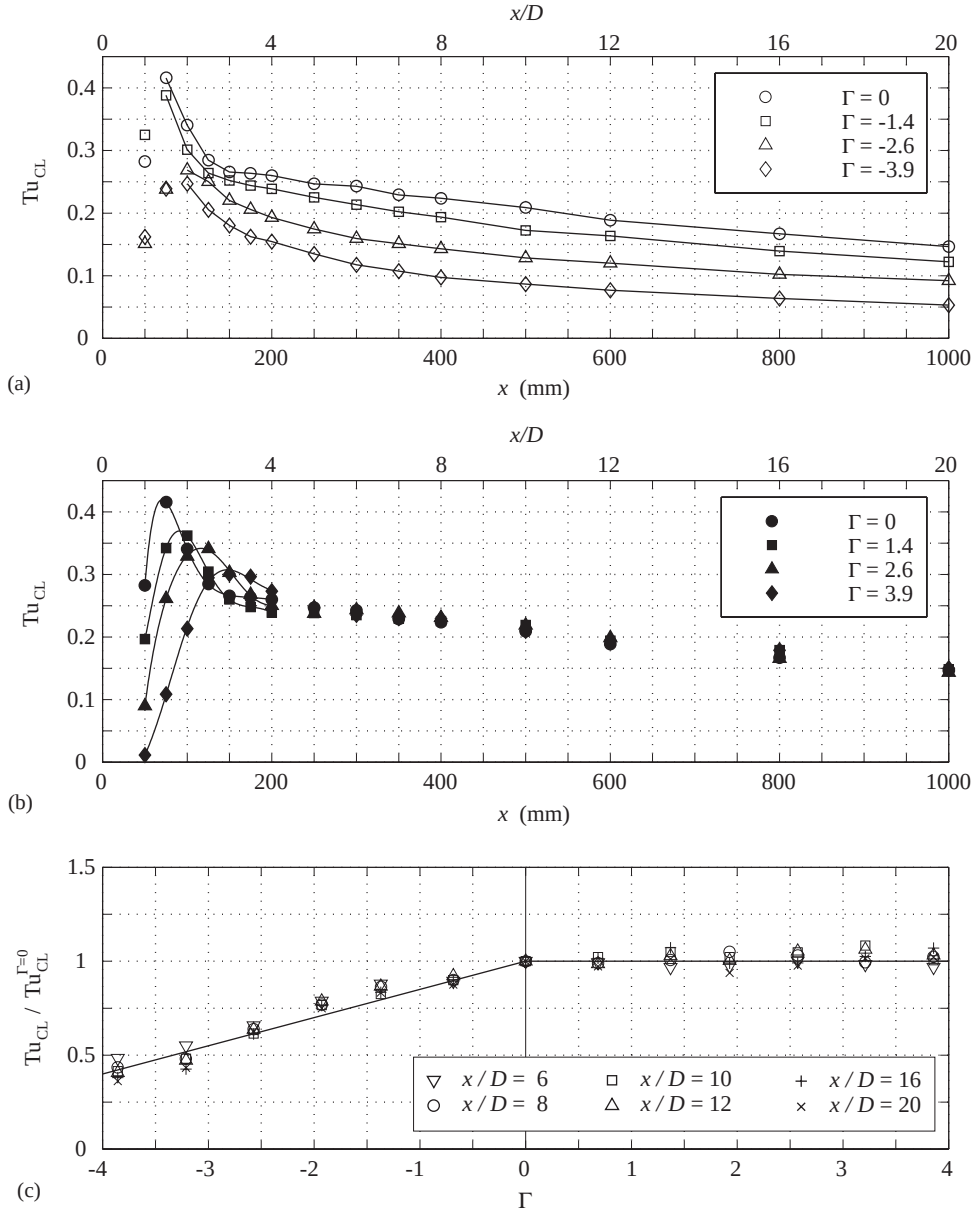

Fig. 8. Tu_{CL}-distribution on the centreline (CL) behind the cylinder. (a) and (b) show the effect of increasing suction and blowing, respectively, inside the wake. (c) shows how the suction decays with $Tu_{CL}^{\Gamma=0}$ and the independence of the blowing for $Tu_{CL}^{\Gamma=0}$.

In Fig. 10(b) all Re are plotted together, however there is a small Re-dependence which can be illustrated by normalizing St with $St_{\Gamma=0}$, as done in Figs. 11(a) and (b) for the suction and blowing cases, respectively. It can be observed that in the suction case the Re-dependence is quite weak, whereas it is somewhat stronger for the blowing case. For large suction the frequency peak of the vortex shedding in the power spectra is strongly reduced and is no longer a dominating frequency. The drop observed in Fig. 11(a) is due to the fact that lower frequencies are detected with more energy content, and these are omitted in Fig. 10(b). Already at moderate ($\Gamma \approx +5$–6) levels of blowing and low Reynolds number (Re = 8500) it is possible to discern the beginning of the saturation level reported by Mathelin et al. (2001b), which is reached at $\Gamma \approx +10$. In the case of blowing the Re-dependence was first noted by Mathelin et al. (2001b), which in the present Γ-investigation is quite small and considered to have a negligible effect in the outcome of the effective-Reynolds number analysis presented here.

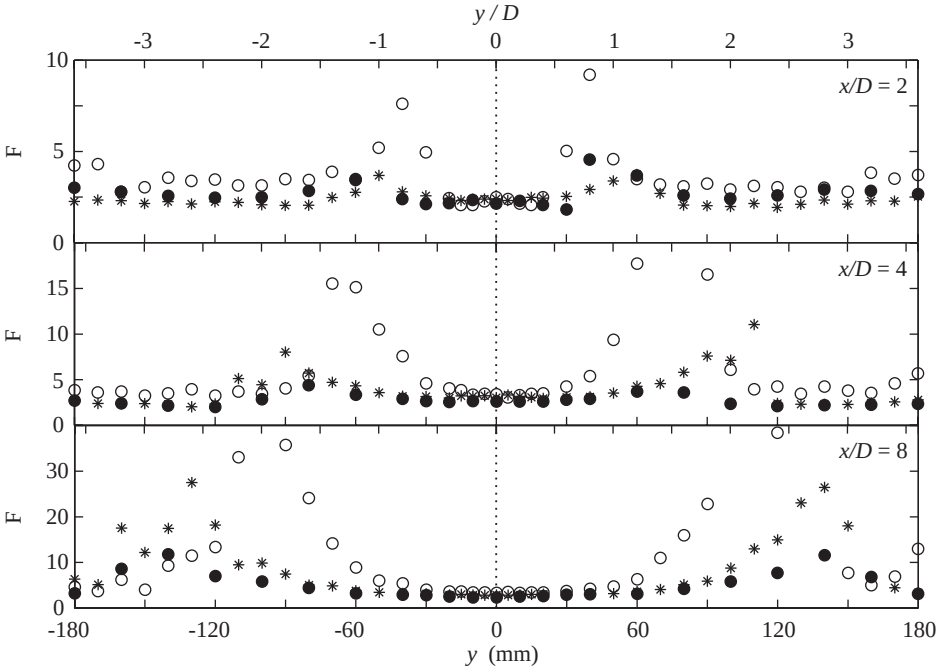

Fig. 9. The flatness distribution across the wake is shown for different x/D-positions. The different symbols corresponds to the normal, the suction, and the blowing case. (✻,○,●) stands for $\Gamma = (0, -2.6, +2.6)$, respectively.

3.5. Drag enhancement/reduction

The momentum equation can be used to calculate the drag coefficient (C_D) from the velocity distribution across the far wake (i.e., for large values of x/D) according to

$$C_D = \frac{4}{D}\int_{y_1}^{y_2} \frac{(U_f - u)u}{U_f^2}\,\mathrm{d}y, \tag{4}$$

where $y_2 - y_1$ is the wake width. This was made for different Γ-values and the result is plotted in Fig. 12 with (○)-symbols. The use of the momentum equation (Eq. (4)) to calculate the total drag can render significant errors if the measured velocity data are too close to the cylinder. At $x/D = 30$ the pressure gradient effects are negligible and the positive contribution of the Reynolds normal stresses to the total drag ceases. Farther downstream the normal stress, instead, gives a small negative contribution (cf. Antonia and Rajagopalan, 1990 for details). However, in all the present drag measurements the x/D-positions were beyond 15, which would in the case of $\Gamma = 0$ render an error that is smaller than 8% [see Antonia and Rajagopalan (1990)]. At $x/D = 20$ the error is less than 5%.

The shape of the drag distribution versus Γ may be compared with that obtained for different Reynolds numbers in the case of a solid cylinder; [see, e.g., Schlichting and Gersten (2000) (p. 19, Fig. 1.12, experimental data from Wieselsberger)]. Now, by applying Eq. (3) interpolated data from Wieselsberger are mapped into Fig. 12 with (●)-symbols. The figure suggests that the blowing/suction rate can be replaced with an effective Reynolds number through Eq. (3), and this relation is valid in a large range of Reynolds numbers (i.e., $\mathrm{Re} \sim 10^2 - 10^6$). Due to a limited length of the wind tunnel there is a mismatch of the data, e.g., one would expect a collapse of the data for $\Gamma = 0$ and $\mathrm{Re} \approx 8300$ which is not the case. The drag coefficient approaches a saturation level for increasing x/D, and in the present case (suction: $x/D = 20$; blowing: $x/D = 16$) one can observe that the saturation level is not yet reached. The two data-sets have an excellent qualitative agreement, only a shift (correction) of the absolute values is needed for total collapse, our C_D-value at $\Gamma = 0$ is 13% lower than the corresponding value of Wieselsberger in Fig. 12. However, the drop on the absolute level of C_D at $\Gamma \approx -2.5$ seems to be the same, and one reason for this collapse could be the fact that the flow situation is different and a smaller x/D is needed to reach the saturation level of C_D. The drop is related to the shift of the separation point as described previously in connection with Fig. 3, which is also present for high Reynolds numbers ($\mathrm{Re} \sim 10^5$) due to the laminar-turbulent boundary layer transition. Both the turbulent profile and

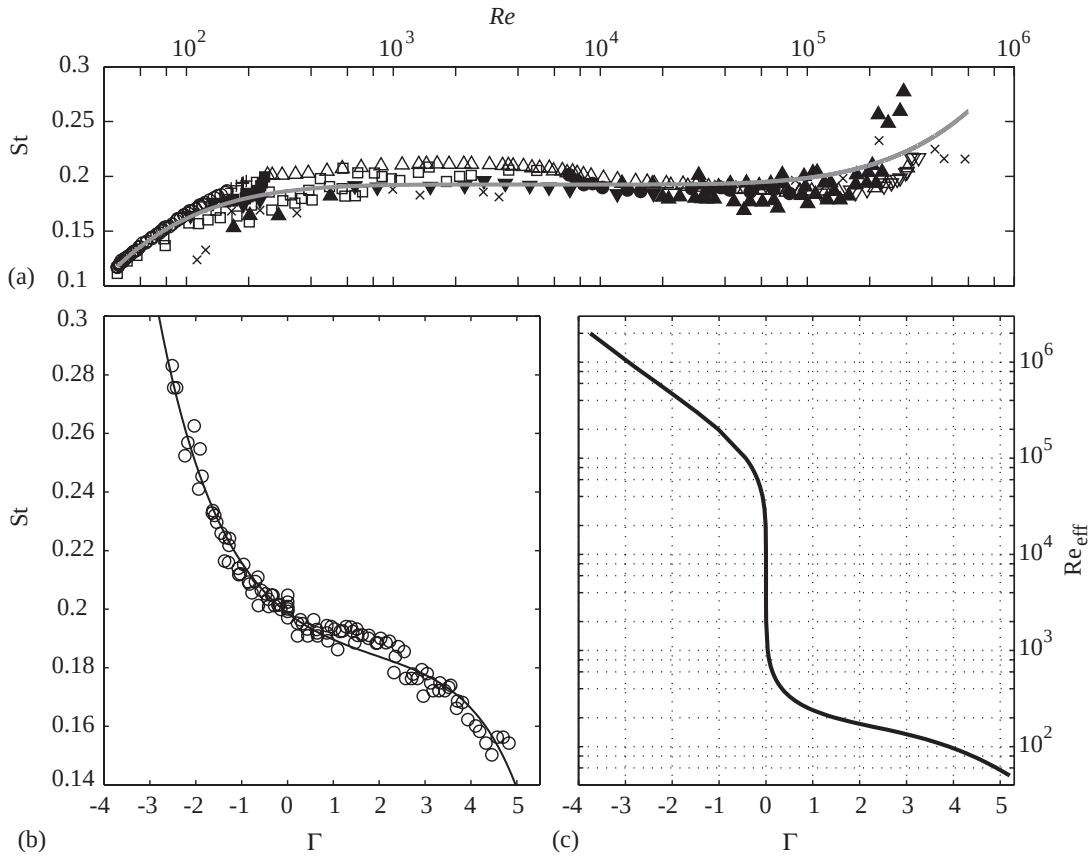

Fig. 10. (a) and (b) show the Strouhal number (St) effect on Reynolds number (Re) and blowing/suction (Γ), respectively. (a) Are data taken from: (○, ■, △) Norberg, (+) Posdziech, (▽) Bearman, (×) Drescher, (●) Etkin et al. (▲) Relf, () Strouhal, (□) Tyler; see text for references. The line is the curve fit given by Eq. (1). (b) Present data (where both U_∞ and V were varied). (c) Shows the effective Reynolds number ($\mathrm{Re}_{\mathrm{eff}}$) vs. Γ (cf. Eq. (3)).

Table 1
The parameter values in Eqs. (1)–(3)

a	b	c	d	e	m	n	k	σ	ΔS
−0.6907	0.9423	289.5	0.1821	−2.309	0.1925	0.0019	−3.744	5	−0.0062

the fuller laminar profile due to suction are more resistant to separation which is the actual cause for the shift. The drag coefficient was also calculated by direct integration of the pressure distribution (cf. Fig. 3a) and is plotted with (△)-symbols in Fig. 12. The agreement with the C_D-value calculated through Eq. (4) is good, which is expected, since the friction contribution to the total drag can be estimated to be only a few percent at this $\mathrm{Re} = 8300$ [cf. p. 92, Fig. 4.15 in Zdravkovich (1997)]. Note that the difference becomes significant for lower Reynolds numbers (or positive values of Γ), which is in concordance with the expected variation of C_D as $\mathrm{Re}^{-1/2}$.

In Fig. 13 the effective diameter (connected to the effective Reynolds number) is used to plot and compare the profiles at the same x/D_{eff}. For $x/D_{\mathrm{eff}} = 8$ one achieves the x-positions 363, 400, and 569 mm for the blowing, the normal, and the suction case, respectively. Fig. 13(b) shows the profiles at $x = 400$, 400, and 600 mm (which are the ones measured closest to the desired locations) for the blowing, the normal and the suction case, respectively, and it is clear from the figure that the appropriate profile scaling has been found. The difference is small in the mean velocity profile, which is the reason why the u_{rms}-profiles have been chosen to be displayed here.

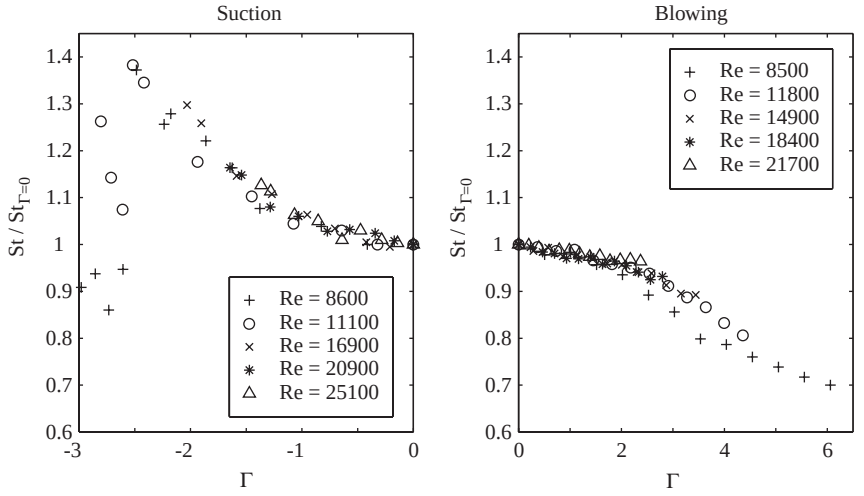

Fig. 11. (a) and (b) show the Strouhal number (St) effect on Reynolds number (Re) with blowing and suction, respectively.

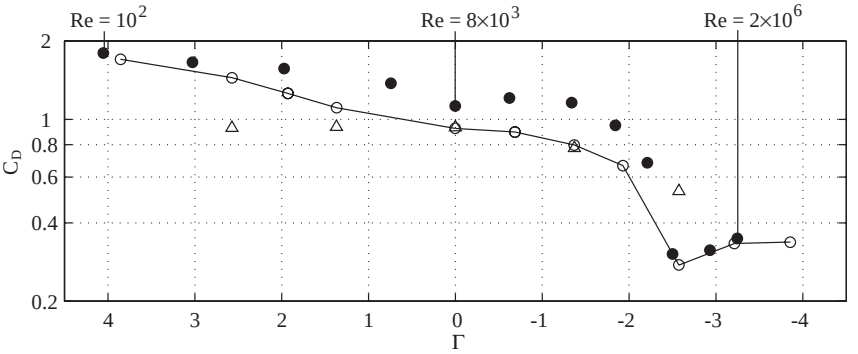

Fig. 12. Shows the effect of C_D when blowing or suction is applied. (○)-symbols and (△)-symbols are calculated using Eq. (4) and by direct integration of the pressure distribution in Fig. 3(a), respectively. (●)-symbols are data from *Wieselsberger* mapped through Eq. (3) using Re = [100, 140, 180, 280, 8000, $10^5 : 10^5 : 10^6$, 2×10^6], which corresponds to the symbols from left to right (see text for reference).

4. Flow visualizations of the near wake

Flow visualization images were taken close behind the cylinder in the near wake. The Reynolds number was Re = 3300 with $U_\infty = 1\,\mathrm{m/s}$, since for higher velocities the smoke generation technique introduces its own shedding disturbances, and the range of Γ investigated was $-5 < \Gamma < +5$ for these flow visualizations. In Fig. 14 instantaneous flow visualization images are shown for five different values of Γ, namely $0, \pm 2.6$ and ± 5.0. These images verify the previously presented measurement results, i.e., with suction the wake shrinks and with blowing it enlarges. In addition, they are able to provide size information of the small eddies formed in the very near wake, and the extent of the vortex formation length.

As the instantaneous images all are unique, it is not possible to draw any firm conclusion about the physical behaviour of the flow from inspection of one image. Therefore, 200 images were digitally averaged for each Γ studied (13 different cases), to be able to extract quantitative information of the vortex formation length. A typical averaged image is shown in Fig. 15(a). The settings (such as contrast and shading) of the averaged images were then all equally changed for a clearer image view. The asymmetry of the image is due to the shading by the cylinder of the light coming from the left-hand side in the figure. The same contour line (corresponding to a chosen value of the light intensity) of the averaged images was then analysed, and in Fig. 15(a) the result of the image averaging (and its contour line) of the

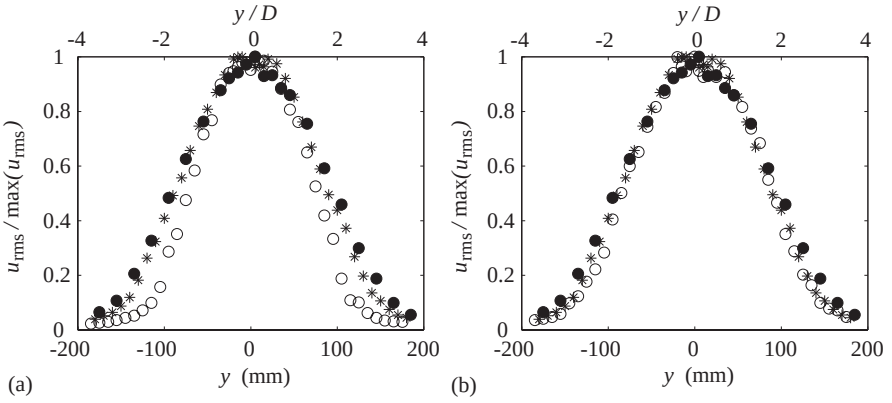

Fig. 13. Shows that the u_{rms}-profiles scales with the effective diameter related to the effective Reynolds number. (✱,○,●) denotes $\Gamma = (0, -2.6, +2.6)$. In (a) $x/D = 8$ for all three cases, and in (b) (✱,●) are shown at $x/D = 8$ and (○) at $x/D = 12$, respectively.

$\Gamma = 0$ case is shown. In Fig. 15(b) the contour lines for $\Gamma = +5, +3.9, +3.2, +2.6, \pm 1.9, \pm 1.4$, and 0 are plotted with alternately dash-dotted and solid lines for increasing $|\Gamma|$. The intersection of the contour lines with the streamwise axis (dotted line in Fig. 15(b)) has been chosen to represent the vortex formation length (L_F); this is plotted versus Γ in Fig. 15(c) with (○)-symbols. The resulting estimation of the vortex formation length is, however, strongly affected by the value of the chosen contour line, but the relative changes on the position is still informative.

Usually the peak of the velocity fluctuation level ($\mathrm{Tu} = u_{rms}/U_\infty$) downstream of the cylinder is used as a definition of the vortex formation length [see e.g., Williamson (1996)]. Therefore, the value of the contour line was here chosen to match $L_F = 80$ mm extracted from Fig. 8(b) in the $\Gamma = 0$ case. Note that the Reynolds number is not the same in the two cases (measurements and visualizations), but are, nonetheless, in the same flow regime. The absence of contour lines for $\Gamma = -2.6, -3.2, -3.9$ and -5 in Fig. 15(b) is due to the fact that the smoke is too dense, because of the wake reduction (cf. Fig. 14), and there will not be any visible lines for the chosen contour value. However, by applying another value of the contour line one obtains the tiny (□)-symbols in Fig. 15(c). Then the three values of $\Gamma = 0, -1.4$ and -1.9 are shifted by an average distance ΔL to collapse with the ○-symbols for the same Γ (i.e., the first chosen value of the contour lines). The same shift ΔL is then applied to the other data as well, to give the large (□)-symbols in Fig. 15(c).

The data in Fig. 15(c) clearly show how the vortex formation length decreases with increasing suction and vice versa for blowing. The data show an almost linear decrease with Γ although L_F is lower for $\Gamma = -1.37$ than for -1.93. This is most probably connected to the complicated mean flow behaviour with suction discussed previously (cf. Section 3.3). Furthermore, for $\Gamma = -5$ (maximum suction investigated) it seems that the wake has disappeared since the vortex formation length obtained is at the cylinder edge (cf. Fig. 15(c)).

Verification of the relative increase of L_F obtained from the flow visualization can be done using the hot-wire measurements. For the blowing case, in Fig. 8(b), the peak appears very distinct and moves from $x/D \approx 1.5$ to 3 with an increase of Γ from 0 to +3.9. Using the values extracted from the flow visualization images one observes an L_F-increase to $x/D \approx 3.5$ in the same blowing interval, which is deemed acceptable considering the resolution in Fig. 8(b).

5. Summary

The flow around a porous cylinder subject to continuous suction or blowing has been experimentally studied for Reynolds numbers of the order of 10^4. It is shown that even moderate levels of the secondary flow, i.e., $\lesssim 5\%$ of the oncoming streamwise velocity, have a large impact on the flow around the cylinder, both for suction and blowing.

Strong enough suction moves the separation line to the rear part of the cylinder in a similar way as it does when the cylinder boundary layer becomes turbulent (resulting in a narrower wake). This is shown in a qualitative way through the drastic reduction of C_D (up to 70%) above a specific value of Γ (≈ -2.5) and by a direct check of the C_p-distribution. When blowing is applied the separation point moves to smaller angles and the drag is shown to increase linearly with increasing magnitude of blowing. Correspondingly, this is shown to result in a widening of the wake.

A measure of the vortex formation length has been defined from flow visualization images and used for investigating relative changes of this length when suction or blowing is applied. For instance, the vortex formation length is decreased

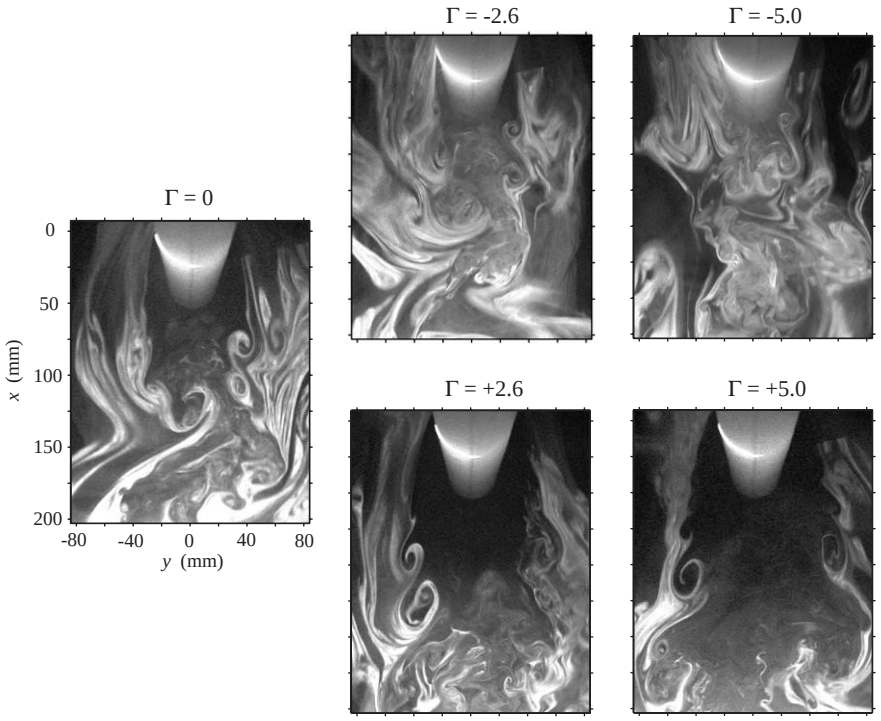

Fig. 14. Instantaneous flow visualization images in the near wake of a porous cylinder subject to continuous suction or blowing for Re = 3300.

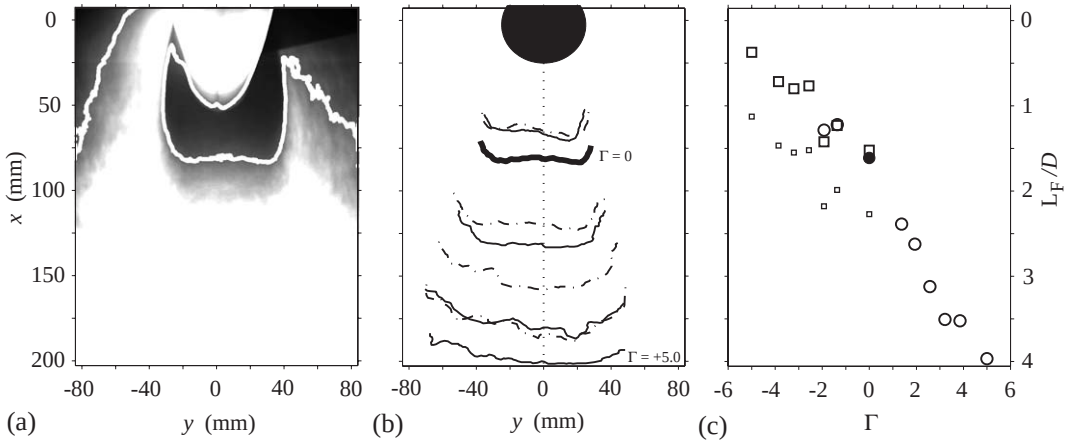

Fig. 15. Variation of the vortex formation length versus Γ. (a) Digital averaging of 200 images for $\Gamma = 0$ with the chosen color contour line. (b) The contour lines for some values of $\Gamma = (+5, +3.9, +3.2, +2.6, \pm 1.4, \pm 1.9, 0)$. Bold solid line corresponds to $\Gamma = 0$ whereafter the contour lines are plotted alternately with dash-dotted and solid lines for increasing $|\Gamma|$. (c) Vortex formation length versus Γ. (○)-symbols corresponds to the intersection points of the contour lines in (b) with the centreline. (●) belongs to $\Gamma = 0$ (see text for (□)-symbols).

by 75% and increased by 150% for $\Gamma \approx -5$ and $+5$, respectively. For the suction case the decrease in formation length may be directly coupled to the rearward motion of the separation point and vice versa for the blowing. It is notable that the turbulence on the wake centreline decreases throughout the whole measured downstream distance ($x/D = 20$) if suction is applied on the cylinder, whereas there is hardly any effect from blowing beyond $x/D = 5$.

The Strouhal number decreases with blowing (around 25% for $\Gamma \approx +5$), whereas suction has the opposite effect (increase of around 50% for $\Gamma \approx -2.5$). Note that uniform suction from the base of a blunt trailing-edge body, interestingly, gives the opposite behaviour [cf. Hammond and Redekopp (1997)], which probably means that the influence of boundary layer is more important than the bleed effect. This can be seen to be coupled to an apparent diameter of the cylinder, which is decreased for suction and increased for blowing as compared to the physical cylinder diameter.

However, another interpretation of the change of Strouhal number is that the effective Reynolds number changes with suction and blowing. In fact it was shown that it was possible to find a relation between an effective Reynolds number and the blowing/suction rate. This relation was verified in a large Reynolds number range ($\mathrm{Re} \sim 10^2 - 10^6$). A weakness of this analysis is that the vortex shedding measurements used for the curve fit according to Eq. (1) are collected in the Re-range $8.5–25 \times 10^3$, and one could question if the same result would have been obtained in another Re-range. The results by Arcas and Redekopp (2004) show that the critical c_q for which vortex shedding is suppressed asymptotes to a constant value with increasing Re (reached at $\mathrm{Re} \approx 1000$), and they argue that this effect is independent of wake flow. This supports our assumption that there is only a week Re dependence with Γ and only "noteable" for base Reynolds numbers less than 1000. Finally, the current effective Re-relation is believed to be suitable as a first estimation in engineering work, but has to be verified at lower/higher Reynolds numbers in future works before one can be sure of its appropriateness.

Acknowledgements

The authors would like to thank Prof. A. Bottaro for hosting the experiment in Toulouse and for valuable comments on the manuscript. We also want to thank Mr Ulf Landén at KTH Mechanics for his skilful construction work of the cylinders. The work is part of a large research program "Control and modelling of turbulent and transitional flows" supported by the Swedish Research Council (VR). J.H.M. Fransson's six-month stay in Toulouse was supported by an EU Marie Curie Training Site Fellowship. P. Konieczny's three-month stay in Stockholm was supported by IMFT and KTH.

References

Antonia, R.A., Rajagopalan, S., 1990. Determination of drag of circular cylinder. AIAA Journal 28, 1833–1834.

Arcas, D.R., Redekopp, L.G., 2004. Aspects of wake vortex control through base blowing/suction. Physics of Fluids 16, 452–456.

Bearman, P.W., 1967. On vortex street wakes. Journal of Fluid Mechanics 28, 625–641.

Berger, E., 1967. Suppression of vortex shedding and turbulence behind oscillating cylinders. Physics of Fluids 10, S191–S193.

Buresti, G., 1998. Vortex shedding from bluff bodies. In: Riera, J.D., Davenport, A.G. (Eds.), Proceedings of the Jubileum Conference on Wind Effects on Buildings and Structures. Porto Alegre, Brazil, 25–29 May, A.A. Rotterdam, Balkema, pp. 61–95.

Cantwell, B., Coles, D., 1983. An experimental study of entrainment and transport in the turbulent near wake of a circular cylinder. Journal of Fluid Mechanics 136, 321–374.

Fransson, J.H.M., Alfredsson, P.H., 2003. On the disturbance growth in an asymptotic suction boundary layer. Journal of Fluid Mechanics 482, 51–90.

Glezer, A., Amitay, M., 2002. Synthetic jets. Annual Review of Fluid Mechanics 34, 503–529.

Hammond, D.A., Redekopp, L.G., 1997. Global dynamics of symmetric and asymmetric wakes. Journal of Fluid Mechanics 331, 231–260.

Hannemann, K., Oertel, H., 1989. Numerical simulation of the absolutely and convectively unstable wake. Journal of Fluid Mechanics 199, 55–88.

Hurley, D.G., Thwaites, M.A., 1951. An experimental investigation of the boundary layer on a porous circular cylinder. British Aeronautical Research Council, Reports and Memoranda No. 2829.

Kármán, T., 1912. Über der Mechanismus des Wiederstandes, den ein bewegter Körper in einer Flüssigkeit erfährt. Göttingen Nachrichten, Mathematisch-Physikalische Klasse, 547–556.

Kiya, M., Suzuki, Y., Arie, M., Hagino, M., 1982. A contribution to the free-stream turbulence effect on the flow past a circular cylinder. Journal of Fluid Mechanics 115, 151–164.

Lindgren, B., Johansson, A.V., 2002. Design and evaluation of a low-speed wind-tunnel with expanding corners. TRITA-MEK Technical Report 2002:14, KTH, Stockholm.

Mathelin, L., Bataille, F., Lallemand, A., 2001a. Near wake of a circular cylinder submitted to blowing—I: Boundary layers evolution. International Journal of Heat and Mass Transfer 44, 3701–3708.

Mathelin, L., Bataille, F., Lallemand, A., 2001b. Near wake of a circular cylinder submitted to blowing—II: Impact on the dynamics. International Journal of Heat and Mass Transfer 44, 3709–3719.

Norberg, C., 1994. An experimental investigation of the flow around a circular cylinder: influence of aspect ratio. Journal of Fluid Mechanics 258, 287–316.

Norberg, C., 2003. Fluctuating lift on a circular cylinder: review and new measurements. Journal of Fluids and Structures 17, 57–96.

Pankhurst, R.C., Thwaites, M.A., 1950. Experiments on the flow past a porous circular cylinder fitted with a Thwaites flat. British Aeronautical Research Council, Reports and Memoranda No. 2787.

Park, D.S., Ladd, D.M., Hendricks, E.W., 1994. Feedback control of von Karman vortex shedding behind a circular cylinder at low Reynolds numbers. Physics of Fluids 6, 2390–2405.

Roshko, A., 1955. On the wake and drag of bluff bodies. Journal of the Aeronautical Sciences 22, 124–132.

Roshko, A., 1961. Experiments on the flow past a circular cylinder at very high Reynolds number. Journal of Fluid Mechanics 10, 345–356.

Roussopoulos, K., 1993. Feedback control of vortex shedding at low Reynolds number. Journal of Fluid Mechanics 248, 267–296.

Schlichting, H., Gersten, K., 2000. Boundary Layer Theory, 8th Edition. Springer, New York.

Shiels, D., Leonard, A., 2001. Investigation of a drag reduction on a circular cylinder in rotary oscillation. Journal of Fluid Mechanics 431, 297–322.

Strouhal, V., 1878. Über eine besondere Art von Tonerregung. Annalen für Physik und Chemie, New Series 5, 216–251.

Szepessy, S., Bearman, P.W., 1992. Aspect ratio and end plate effects on vortex shedding from a circular cylinder. Journal of Fluid Mechanics 234, 191–217.

Tokumaru, P.T., Dimotakis, P.E., 1991. Rotary oscillation control of a cylinder wake. Journal of Fluid Mechanics 224, 77–90.

Wang, A.-B., Travnicek, Z., Chia, K.-C., 2000. On the relationship of effective Reynolds number and Strouhal number for the laminar vortex shedding of a heated circular cylinder. Physics of Fluids 12, 1401–1410.

Williamson, C.H.K., 1996. Vortex dynamics in the cylinder wake. Annual Review of Fluid Mechanics 28, 477–539.

Wood, C.J., 1967. Visualization of an incompressible wake with base bleed. Journal of Fluid Mechanics 29, 259–272.

Zdravkovich, M.M., 1997. Flow around circular cylinders, vol 1: Fundamentals. Oxford University Press, Oxford.

Zdravkovich, M.M., 2003. Flow around circular cylinders, vol 2: Applications. Oxford University Press, Oxford.